OPEN ACCESS
IOP Publishing
Superconductor Science and Technology
Supercond. Sci. Technol. **34** (2021) 035031 (8pp)
https://doi.org/10.1088/1361-6668/abdedf

Resistivity, Hall effect, and anisotropic superconducting coherence lengths of $HgBa_2CaCu_2O_6$ thin films with different morphology

H Richter[1], W Lang[1], M Peruzzi[2], H Hattmansdorfer[2], J H Durrell[2,3] and J D Pedarnig[2]

[1] Faculty of Physics, University of Vienna, Boltzmanngasse 5, A-1090 Wien, Austria
[2] Institute of Applied Physics, Johannes-Kepler-Universität Linz, A-4040 Linz, Austria
[3] Engineering Department, University of Cambridge, Trumpington Street, Cambridge CB2 1PZ, United Kingdom

E-mail: wolfgang.lang@univie.ac.at

Received 16 July 2020, revised 15 January 2021
Accepted for publication 22 January 2021
Published 8 February 2021

Abstract

Thin films of the high-temperature superconductor $HgBa_2CaCu_2O_6$ have been prepared on $SrTiO_3$ substrates by pulsed-laser deposition of precursor films and subsequent annealing in mercury-vapor atmosphere. The microstructural properties of such films can vary considerably and have been analyzed by x-ray analysis and atomic force microscopy. Whereas the resistivity is significantly enhanced in samples with coarse-grained structure, the Hall effect shows little variation. This disparity is discussed based on models for transport properties in granular materials. We find that, despite of the morphological variation, all samples have similar superconducting properties. The critical temperatures $T_c \sim 121.2$ K …122.0 K, resistivity, and Hall data indicate that the samples are optimally doped. The analyses of superconducting order parameter fluctuations in zero and finite magnetic fields yield the in-plane $\xi_{ab}(0) \sim 2.3$ nm …2.8 nm and out-of-plane $\xi_c(0) \sim 0.17$ nm …0.24 nm Ginzburg–Landau coherence lengths at zero temperature. Hall measurements provide estimates of carrier scattering defects in the normal state and vortex pinning properties in the superconducting state inside the grains.

Keywords: mercury cuprate, superconductor, resistivity, Hall effect, order parameter fluctuations, coherence length, granular materials

(Some figures may appear in colour only in the online journal)

1. Introduction

The mercury cuprates of the Hg–Ba–Ca–Cu–O family form a homologous series with the chemical formula $HgBa_2Ca_{n-1}Cu_nO_{2n+2+\delta}$ (HBCCO). The discovery of high-temperature superconductivity in the $n = 1$ compound [1] and the even higher transition temperatures $T_c = 120$ K in the $n = 2$ [2] and $T_c = 135$ K in the $n = 3$ material [3], respectively, has triggered enormous research interest. The latter compound still holds the record for the highest critical temperature T_c of any superconductor at ambient pressure and for a cuprate superconductor with $T_{c,\mathrm{onset}} = 164$ K under quasi-hydrostatic pressure of 31 GPa [4]. Mercury cuprates have been synthesized from $n = 1$ to 7 with T_c raising with the number n of neighboring CuO_2 layers up to a maximum at $n = 3$ and then decreasing for $n > 3$ [5].

In contrast to their very promising superconducting properties, the mercury cuprates are hard to synthesize and handle due to the highly volatile and toxic nature of Hg and Hg-based compounds. For a possible effective use, but also for a measurement of the basic intrinsic properties, the fabrication of high-quality thin films is demanded. Several groups have succeeded in this task, mainly by using pulsed-laser deposition (PLD) of a precursor film with subsequent annealing in Hg and O_2 containing atmosphere [6–9]. Later it was demonstrated that HBCCO thin films can be grown on vicinal substrates in a well-oriented manner and form a roof-tile like structure that allows for measurements of in-plane and out-of-plane properties on the very same sample [10, 11].

As a consequence of the subtle preparation conditions, the properties of HBCCO samples reported by various groups vary significantly. Investigations of the electrical transport properties in samples with different structural properties have been rare. It remains ambiguous whether such diversity stems from slightly different preparation conditions in individual laboratories or can occur also at supposedly identical fabrication procedures. For instance, in polycrystalline samples of $HgBa_2CaCu_2O_6$ (Hg-1212) a room temperature variation of the electrical resistivity by a factor larger than two was observed between individual samples that were cut from the same ceramics but annealed for different time intervals [12]. Surprisingly, the Hall effect of these samples was remarkably similar. On the other hand, both the resistivity and the Hall effect changed significantly in a Hg-1212 thin film after several annealing steps in different mercury and oxygen atmospheres [13].

Several authors have investigated the electrical transport properties, such as resistivity and the Hall effect, in HBCCO in detail, but without putting emphasis on possible variations between individual samples. Mostly, results of only a single sample were presented. In the mixed-state Hall effect, a double sign reversal, similar to that observed in other cuprate superconductors with high anisotropy, was reported [14]. In addition, it was found that after introducing strong pinning by high-energetic Xe^+ ion irradiation, a triple sign change evolves [15]. Further investigations concerned the resistivity in magnetic fields oriented perpendicular and parallel to the CuO_2 planes, the critical current density, the angular dependence of the depinning field [16] and the normal and mixed-state Hall effect [17] in partially Re-substituted $Hg_{0.9}Re_{0.1}Ba_2CaCu_2O_{6+\delta}$ (HgRe-1212) thin films. The Hall effect's dependence on the angle between the magnetic field and the *ab* planes in the Hg-1212 thin films could be explained by the common behavior of HTSCs in the normal state and a renormalized superconducting fluctuation model for the temperature region close to T_c, where the Hall effect exhibits its first sign change [18].

Recently, revived interest in the $n = 1$ HBCCO compound has emerged, as it is a model system for a single-CuO_2 layer cuprate. Investigations on underdoped samples of this compound [19, 20] have shed light on the nature of the ubiquitous pseudogap in underdoped cuprate superconductors.

In this paper we investigate the structural and the electrical transport properties of three Hg-1212 thin films, fabricated by pulsed-laser deposition on $SrTiO_3$ substrates. Although we intentionally included a 'bad' sample with much higher room-temperature resistivity, we find that fundamental superconducting properties, like the critical temperature and the anisotropic Ginzburg–Landau coherence lengths show only little variation in samples with significantly different granularity.

2. Sample preparation and characterization

Thin films of Hg-1212 were fabricated in three individual runs (each about four months apart) under the same preparation conditions. The labeling of the samples corresponds to the time sequence. The fabrication is a two-step process using polished 5×5 mm large (001) $SrTiO_3$ crystal substrates with similar surface roughness. Firstly, amorphous precursor films were deposited on the substrates using pulsed-laser deposition (PLD) [21] with 25 ns KrF excimer laser pulses ($\lambda = 248$ nm) with 10 Hz repetition rate. In a second step, the films were annealed in a mercury vapor atmosphere employing the sealed quartz tube technique [8–10]. Typically, sintered targets of nominal composition Ba:Ca:Cu = 2:2:3 are employed for laser ablation and precursor films are deposited at room temperature. For Hg-1212 phase formation and for crystallization of films with *c*-axis orientation annealing at high temperature (800 °C–830 °C) and high vapor pressure (35 bar) is required. HBCCO thin films usually reveal reduced surface quality, phase purity and crystallinity as compared to other HTSC thin films that are grown in a single-step process, like those of $YBa_2Cu_3O_7$ (YBCO) and $Bi_2Sr_2Ca_{n-1}Cu_nO_{2(n+2)+\delta}$ (BSCCO). However, phase-pure epitaxial Hg-1212 films with improved surface morphology are achieved by using mercury-doped targets (Hg:Ba:Ca:Cu $\approx$ 0.8:2:2:3) for laser-ablation and by deposition of precursor films at an elevated substrate temperature $T_S = 350$ °C.

Figure 1 shows the x-ray diffraction (XRD) data of three samples. The (00*l*) indices of Hg-1212 are clearly visible. The full width at half maximum (FWHM) of the (005) rocking curve is about 7° for sample A, 6° for sample B, and 1° for sample C, respectively (data not shown). Besides of the well pronounced peaks resulting from the $SrTiO_3$ substrate only small traces of unknown spurious phases are visible and marked by asterisks. In sample B, however, the Hg-1212 XRD peaks have lower heights as compared to those of $SrTiO_3$ and the peaks of spurious phases are larger, indicating a smaller amount of the Hg-1212 phase and a larger portion of spurious phases and voids. This reflects the susceptibility of the mercury cuprates to subtle uncontrollable variations of the preparation conditions, since identical procedures and the same substrate materials have been used.

The surface textures of the three samples are measured by atomic force microscopy (AFM) and are displayed in figure 2. The annealed films reveal a dense and homogeneous structure, an even surface without *a*-axis oriented grains, and no regions of unreacted material. Bright spots in the AFM scans indicate particulates of 3…6 μm diameter and 0.5…1 μm height, which are typically found in HTSC thin films fabricated by

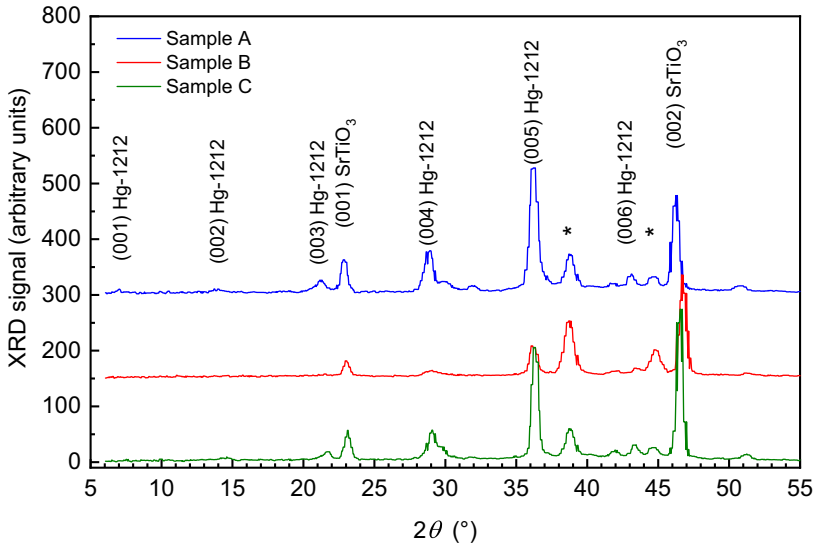

Figure 1. X-ray diffraction scan of three $HgBa_2CaCu_2O_6$ (Hg-1212) thin films. The curves are offset for better visibility (sample A: top curve, sample C: bottom curve). The (00*l*) indices of Hg-1212 and the $SrTiO_3$ substrate are indicated and unknown spurious phases are marked by asterisks. Note the significant reduction of the Hg-1212 peak heights of sample B.

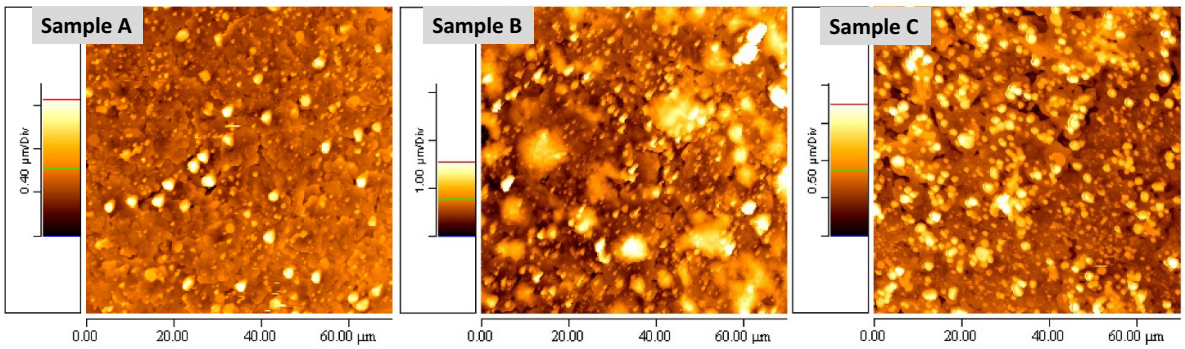

Figure 2. Atomic force microscopy height profiles of samples A, B, and C. All pictures display an area of 70 μm × 70 μm. Bright spots indicate particulates on the film surface.

PLD and, for instance in YBCO, can be removed by mechanical and chemical polishing [22]. Sample B exhibits a coarser grain morphology and the larger angular spread of the x-ray rocking curve indicates an enhanced misorientation of the grains.

3. Experimental setup for the electrical measurements

For the electrical transport measurements, the Hg-1212 films were patterned by standard photolithography and wet-chemical etching into strips with two pairs of adjacent side arms. Electrical contacts were established by Au wire and silver paste on Au pads that were previously evaporated on the sample's side arms. The thicknesses of the films were determined by AFM. The main parameters of the three samples are summarized in table 1.

Resistivity and Hall effect measurements were performed in a closed-cycle cryocooler mounted between the pole pieces of an electromagnet. DC currents were provided by a Keithley 2400-LV constant current source and the longitudinal and transverse voltages were recorded simultaneously with the two channels of a Keithley 2182 nanovoltmeter. The directions of both the current and the magnetic field were reversed multiple times for every data point to cancel spurious thermoelectric signals, transverse voltages stemming from contact misalignment, and to enhance the signal to noise ratio. The temperature stability at individual setpoints is better than ± 0.01 K.

4. Results and discussion

The temperature dependencies of the longitudinal resistivity of the three samples are compared in figure 3. They show a linear behavior of the normal state resistivity ρ_{xx}, typical for optimally-doped cuprate HTSCs and a reduction of ρ_{xx} below the linear trend above T_c stemming from superconducting fluctuations [23].

The inset of figure 3 demonstrates that, despite of the significantly different absolute values of ρ_{xx}, all three samples exhibit a similar qualitative behavior when a scaling according to $\rho_{xx}(T)/\rho_{xx}(300\,\mathrm{K})$ is applied. This fact contrasts with the typical observation in HTSCs with point defects like

Table 1. Properties of the Hg-1212 films, where w is the width of the patterned strip, l the distance between the voltage probes, t_z the film thickness, and T_c the critical temperature defined by the inflection point of the resistive superconducting transition curve. Note that sample A has similar bridge dimensions as the other samples, but different voltage probes have been used. The intercept of the extrapolated linear normal-state resistivity is $\rho_{xx}(0\,\mathrm{K})$, and $\xi_{ab}(0)$ are the in-plane and $\xi_c(0)$ the out-of-plane Ginzburg–Landau coherence lengths at $T = 0$, respectively.

Sample	w (μm)	l (μm)	t_z (μm)	T_c (K)	$\rho_{xx}(0\,\mathrm{K})$ ($\mu\Omega$ cm)	$\xi_{ab}(0)$ (nm)	$\xi_c(0)$ (nm)
A	140 ± 10	620 ± 5	0.41 ± 0.09	122.0	-36	2.4 ± 0.3	0.18 ± 0.05
B	138 ± 2	1240 ± 5	0.46 ± 0.14	121.2	-43	2.3 ± 0.3	0.24 ± 0.05
C	128 ± 6	1240 ± 5	0.43 ± 0.19	121.7	-42	2.8 ± 0.2	0.17 ± 0.02

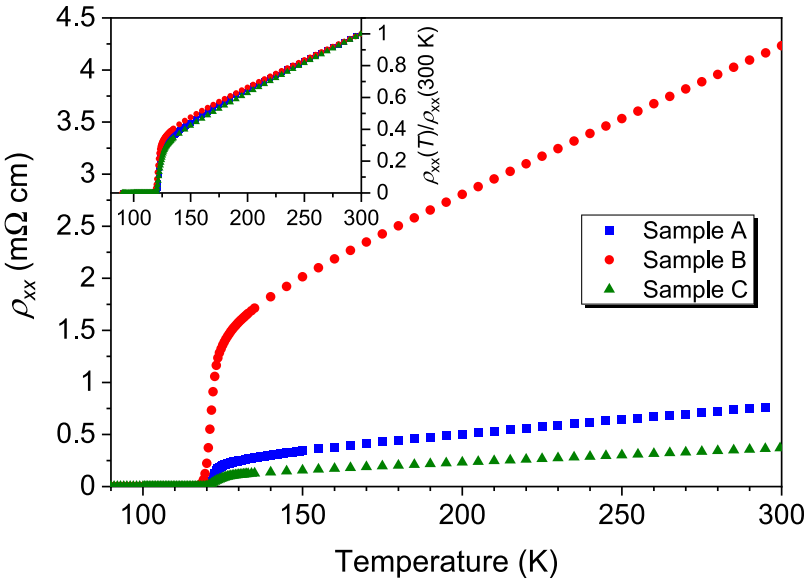

Figure 3. Electrical resistivity of the three Hg-1212 films as a function of temperature. The inset shows the resistivities normalized to their values at 300 K.

disordered oxygen atoms [24, 25], where such a scaling is violated and the intercept $\rho_{xx}(0\,\mathrm{K})$ from an extrapolation of the normal state is shifted to higher values when the concentration of point defects is increased. In fact, $\rho_{xx}(0\,\mathrm{K})$ is slightly negative and similar for all three samples, indicating a minor influence of point defects on the resistivity. Remarkably, the critical temperatures of all samples are similar, too, as listed in table 1. These observations indicate that the intragrain resistivities of the samples are similar, but different granularity and different amount of voids and bad-conducting spurious phases lead to a large variation of the macroscopic resistivity.

An analysis of thermodynamic superconducting order parameter fluctuations (SCOPF) [26] allows one to determine the anisotropic Ginzburg–Landau coherence lengths in superconductors. This method has been applied to many HTSCs but only rarely to Hg-1212 and is based on an evaluation of the paraconductivity $\Delta\sigma_{xx}(0)$ in zero and the paraconductivity $\Delta\sigma_{xx}(B_z)$ in a moderate magnetic field B_z, applied perpendicular to the crystallographic ab plane. The total measured conductivity is $\sigma_{xx}(0) = \sigma^N_{xx}(0) + \Delta\sigma_{xx}(0)$ and $\sigma_{xx}(B_z) = \sigma^N_{xx}(B_z) + \Delta\sigma_{xx}(B_z)$, respectively. Commonly, the normal-state conductivities $\sigma^N_{xx}(0)$ and $\sigma^N_{xx}(B_z)$ are determined by extrapolating the linear temperature dependence of the resistivity in the normal state towards lower temperatures. In our samples no deviations from a linear trend at temperatures between 200 K and 300 K are noticeable and, hence, it is assumed that the SCOPF are negligible above 200 K and furthermore no influence of a pseudogap behavior is expected [27].

In a magnetic field, however, such a procedure requires the assumption that the normal-state magnetoresistance is negligible, i.e. $\sigma^N_{xx}(B_z) \simeq \sigma^N_{xx}(0)$ in the temperature range under investigation [28]. In fact, the parameters for the linear fits to $\sigma_{xx}(B_z)$ and $\sigma_{xx}(0)$ above 200 K are the same, which indicates a negligible normal-state magnetoresistance in all samples.

Several different processes contribute to SCOPF [26], but under the conditions explored in this work, the Aslamazov–Larkin (AL) [29] process dominates by far. The Lawrence–Doniach (LD) model [30] is an appropriate extension for two-dimensional layered superconductors with the out-of-plane Ginzburg–Landau coherence length at $T = 0$, $\xi_c(0)$, as the only one fit parameter. The paraconductivity is given by

$$\Delta\sigma^{\mathrm{LD}}_{xx} = \frac{e^2}{16\hbar d}(1+2\alpha)^{-1/2}\epsilon^{-1}, \qquad (1)$$

where e is the electron charge, $\hbar$ the reduced Planck constant, $d = 1.2665$ nm the distance between adjacent CuO_2 double layers [31], and $\epsilon = \ln(T/T_c) \approx (T - T_c)/T_c$ is a reduced

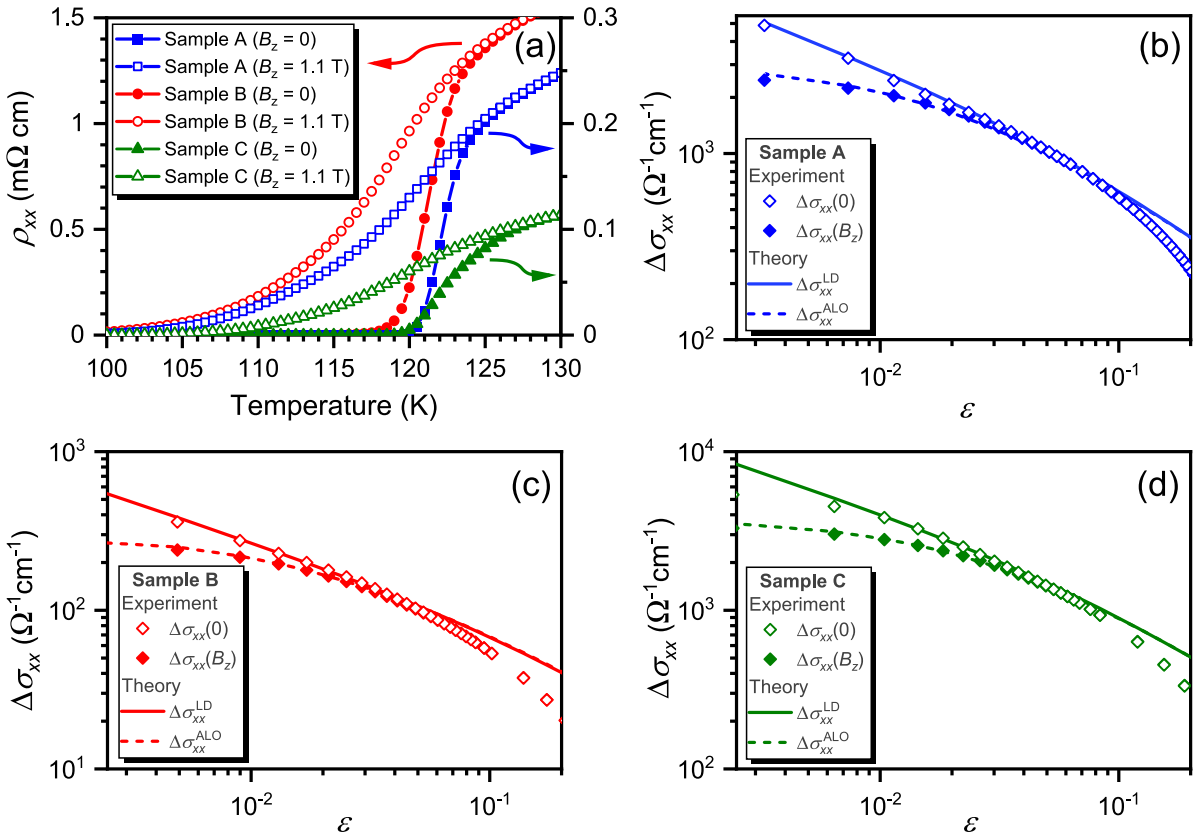

Figure 4. (a) Superconducting transition of the three Hg-1212 films in zero and finite magnetic fields. (b)–(d) Paraconductivities of the samples as a function of the reduced temperature $\varepsilon = \ln(T/T_c)$ in zero magnetic field and in $B_z = 1.1$ T. Symbols indicate the experimental data, full lines the fits to equation (1) for the paraconductivity in zero field and dotted lines the fits to equation (2) in finite field, respectively.

temperature. The dimensionless coupling parameter between the superconducting layers is $\alpha = 2\xi_c^2(0)d^{-2}\epsilon^{-1}$.

A magnetic field oriented perpendicular to the CuO_2 layers leads to a reduction of SCOPF by orbital and Zeeman pair breaking, which is also reflected by a decrease of the mean-field T_c. The Zeeman interaction is important for an orientation of the magnetic field parallel to the CuO_2 layers only [32] and can be neglected in the present analysis. The paraconductivity in finite magnetic field considering the orbital interaction with the AL process (ALO) is [33]

$$\Delta\sigma_{xx}^{\mathrm{ALO}} = \frac{e^2}{8\hbar h^2}\int_0^{2\pi/d} \epsilon_k \left[\psi\left(\frac{1}{2}+\frac{\epsilon_k}{2h}\right) - \psi\left(1+\frac{\epsilon_k}{2h}\right) + \frac{h}{\epsilon_k}\right]\frac{\mathrm{d}k}{2\pi}, \tag{2}$$

where $\epsilon_k = \epsilon[1+\alpha(1-\cos kd)]$, k is the momentum parallel to B_z, ψ is the digamma function, and $h = \ln[T_c(0)/T_c(B_z)] = 2e\xi_{ab}^2(0)B_z/\hbar$ reflects the reduction of T_c in the magnetic field. equation (2) contains two fit parameters, where $\xi_c(0)$ is already determined by equation (1), leaving the in-plane coherence length at $T = 0$, $\xi_{ab}(0)$, as the only adjustable parameter.

Figure 4(a) shows the superconducting transitions in zero and finite magnetic fields and figures 4(b)–(d) the resulting paraconductivities $\Delta\sigma_{xx}(0)$ and $\Delta\sigma_{xx}(B_z)$ as a function of the reduced temperature ε together with fits to the LD (equation (1)) and ALO (equation (2)) processes. To account for the higher resistivities observed in samples A and B due to a larger fraction of non-superconducting voids and spurious phases, the theoretical paraconductivity curves are scaled by a factor of 0.70 (0.09) for sample A (sample B) that is determined during the fit procedure. The choice of the scaling factor and the coherence lengths have only marginal interdependence, since only the latter define the curvature of the plots. Of course, this introduces an additional uncertainty for the evaluation of $\xi_c(0)$ in samples A and B but has only a minor impact on $\xi_{ab}(0)$.

In paraconductivity studies of HTSCs three temperature regions can be distinguished. Very close to T_c the fluctuating superconducting domains start to overlap and the paraconductivity falls below the predictions of equations (1) and (2). This situation is accounted for by renormalized fluctuation theories [34, 35], which do not contribute to the determination of the coherence lengths and hence are outside of the scope of the present analysis. A counteracting effect can be evoked by a non-homogenous T_c [36]. Both corrections, as well as the exact value of the mean-field T_c used for the calculation of the reduced temperature ε are relevant for $\epsilon < 0.01$ only. On the other hand, a high energy cutoff of the fluctuation spectrum [37] leads to a smaller paraconductivity as compared to theory for $\epsilon > 0.1$ that can be modeled by a heuristic function resulting in a very similar $\xi_c(0)$ [38]. In the intermediate temperature region $0.01 < \epsilon < 0.1$ the fit parameters can be determined with good precision.

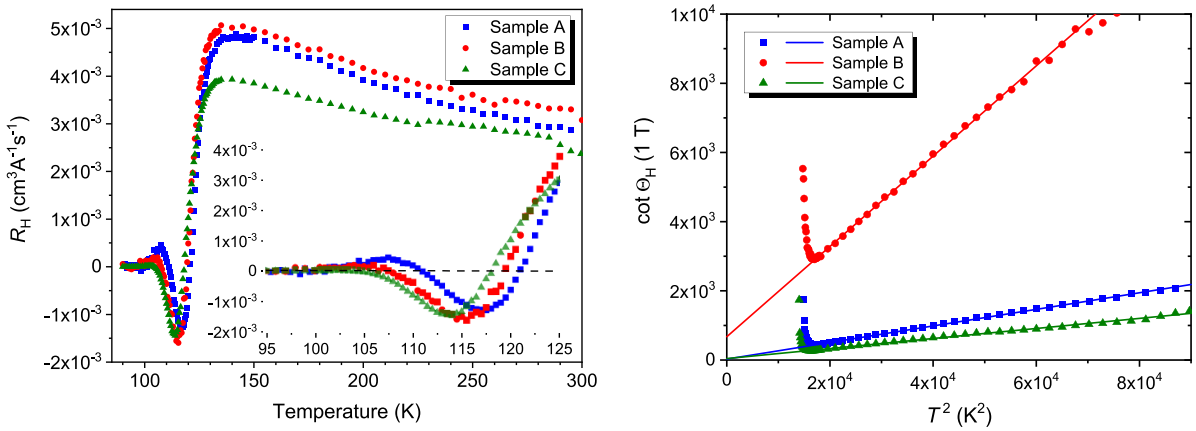

Figure 5. Hall effect in the three Hg-1212 films, measured at $B_z = 1.1$ T. Left panel: Hall coefficient R_H as a function of temperature. The inset shows a blow-up of the temperature region around T_c. Right panel: cotangent of the Hall angle Θ_H normalized to 1 T as a function of the square of the temperature. Only data above T_c are shown. The lines indicate fits to the data in the normal state.

The resulting values of the coherence lengths are listed in table 1. Note that despite of the large variation of the resistivities of the samples, their coherence lengths are quite similar. Nonetheless, a correlation with other sample properties can be discussed tentatively. With degradation of the morphology and increase of the resistivity, $\xi_c(0)$ increases, while $\xi_{ab}(0)$ decreases, leading to a reduction of the anisotropy in the superconducting state. An increase of crystallographic misorientation between individual grains naturally leads to a reduction of the anisotropy, which is here determined averaged over the entire film, and is also evidenced by the broader rocking curves of samples A and B.

Compared to other studies in grain-aligned polycrystalline Hg-1212 samples we find about half as long out-of-plane coherence lengths [39] and larger [39, 40] or similar [41] in-plane coherence lengths, indicating a higher anisotropy $\gamma = \xi_{ab}(0)/\xi_c(0) \sim 9.6 \ldots 16.5$ in our samples. In a HgRe-1212 thin film $\gamma \sim 7.7$ was estimated [16], while higher values $\gamma \sim 29$ [42] and $\gamma \sim 52$ [43] were reported in $HgBa_2CuO_{4+\delta}$ and $HgBa_2Ca_2Ca_2Cu_3O_{8+\delta}$ single crystals, respectively. These findings point to a correlation between sample morphology and measured anisotropy.

The Hall coefficient is $R_H = E_y/(j_x B_z)$, where E_y is the transverse electric field measured between adjacent side arms of the sample, j_x the current density along the strip-shaped Hg-1212 film, and B_z the magnetic field perpendicular to the film surface. Remarkably, R_H is similar in all samples, as can be noticed in figure 5 (left panel).

In the normal state R_H is positive (hole-like) and increases towards lower temperatures, followed by a sharp drop around T_c and a subsequent change to negative values. Furthermore, a second sign reversal back to positive R_H is noticeable, but differently pronounced in the samples as displayed in the inset of figure 5 (left panel). Qualitatively, our observations are in line with previous investigations in Hg-1212 [14, 17] and Bi-2212 films [44, 45]. The peculiar sign change of R_H from positive in the normal state to negative in the vortex-liquid regime is still not consensual [46, 47] and is out of the scope of the present work. Renormalized superconducting fluctuations [48], collective vortex effects [49], and pinning centers [50] are some possible explanations.

While the domain of negative R_H looks similar in all samples, the positive R_H data at the low temperature tail show more variations. In YBCO, such a double sign reversal is rarely observed and then attributed to vortex-lattice melting [51] or pinning at twin boundaries [52]. In Hg-1212 it is considered an intrinsic property [14], like in Bi-2212, where it becomes more prominent when pinning is reduced in enhanced current densities [45]. As it will be discussed below, the Hall effect is dominated by *intragrain* properties. Thus, enhanced vortex pinning within the grains would shift the onset of dissipation and hence the appearance of a finite Hall signal to higher temperatures [48]. Along these lines one might argue that an intrinsic positive Hall effect at the low temperature tail is reduced or invisible in samples with a higher density of vortex pinning centers.

The Hall effect in the normal state is displayed in the right panel of figure 5 in an appropriate scaling to demonstrate that, for all three samples, it follows Anderson's law [53] $\cot\Theta_H = \alpha T^2 + C$, where C is proportional to the density of carrier scattering defects and α is a measure of the carrier density. The linear trend can be observed in the temperature range from ∼135 K to 300 K, up to higher temperatures than in HgRe-1212 thin films [16]. The upturn close to T_c is due to the onset of SCOPF.

At first sight, α and C appear to be quite different. Since $\cot\Theta_H = \rho_{xx}/(R_H B_z)$, the voids in the sample that lead to enhanced ρ_{xx}, as seen in figure 3, in a similar manner effect $\cot\Theta_H$. Hence, if the same scaling as in the inset of figure 3 is applied to the curves of samples A and B, taking sample C as the reference, a comparison can be made. It turns out that α is similar in all samples, reflecting a similar carrier density inside the grains, while the intercept C is largest in sample B and smallest in sample A. Although only a rough estimate, it would indicate the smallest density of carrier scattering defects inside the grains in sample A. Such defects do not only impact the normal-state transport effects but can also act as vortex pinning centers in the superconducting state. On these grounds it

is understandable that in sample A the smallest value of the intercept C and the largest positive Hall effect peak at low temperatures are observed.

Finally, we discuss the minor variation with sample morphology of R_H observed in figure 5 (left panel) to the contrasting large spread of the resistivities (see figure 3). Volger [54] has theoretically considered a material consisting of well conducting grains separated by thin layers of lower conductivity, which in our samples can be attributed tentatively to grain boundaries, voids, and spurious badly conducting phases. In this scenario, the experimentally determined average resistivity can be dominated by the high-resistance domains and can thus be much higher than the intragrain resistivity. On the other hand, the experimentally found R_H will not be very different from its intragrain value.

Alternatively, one could consider that the voids in the material reduce the cross section of the current path. Then, using the macroscopic dimensions of the sample for the calculation, the resistivity will be overestimated. However, the local current density in the grains is larger than its average value, giving rise to an enhanced transverse Hall voltage. Since the Hall voltage is probed quasi-electrostatically, *intergranular* resistances are negligible and the Hall voltages of individual grains add up in a series connection across the width of the thin film. Intuitively, this is also reflected by the calculation of R_H into which only the film thickness enters, whereas for the evaluation of the resistivity the sample's thickness, width, and the probe distance are relevant.

5. Conclusions

In summary, we have investigated the resistivity and the Hall effect in three Hg-1212 thin films of different morphologies, which were characterized by x-ray diffraction and AFM scans. Despite of a large variation of the absolute values, the resistivity of all samples is linear in the normal state, as it is observed in optimally doped HTSCs. The critical temperatures $T_c \sim 121.2\,\mathrm{K}$ …$122.0\,\mathrm{K}$ are similar in all samples, too, and the deviations from the linear resistivity trend due to SCOPF allow for the determination of the in-plane $\xi_{ab}(0) \sim 2.3\,\mathrm{nm}$ …$2.8\,\mathrm{nm}$ and out-of-plane $\xi_c(0) \sim 0.17\,\mathrm{nm}$ …$0.24\,\mathrm{nm}$ Ginzburg–Landau coherence lengths.

In sharp contrast to the resistivity, the normal-state Hall effect is similar in the three samples and is dominated by their intragranular properties. It allows to conclude that inside the grains the carrier density is almost the same in all samples, but the density of carrier scattering defects is different. The Hall effect in the superconducting state exhibits two sign changes, from which the one at lower temperatures is sample dependent and can indicate different vortex pinning properties due to different defect densities inside the grains. Finally, our analyses of various transport measurements on different samples indicate that the intragranular intrinsic properties of the Hg-1212 films can be estimated adequately despite of their diverse macroscopic resistivities.

Acknowledgments

This work was supported by the Austrian Science Fund under Grant Nos I4865-N and P18320-N07 and the COST Actions CA16218 (NANOCOHYBRI) and CA19108 (Hi-SCALE) of the European Cooperation in Science and Technology.

ORCID iDs

W Lang https://orcid.org/0000-0001-8722-2674
J H Durrell https://orcid.org/0000-0003-0712-3102

References

[1] Putilin S N, Antipov E V, Chmaissem O and Marezio M 1993 *Nature* **362** 226–8
[2] Putilin S N, Antipov E V and Marezio M 1993 *Physica* C **212** 266–70
[3] Schilling A, Cantoni M, Guo J D and Ott H R 1993 *Nature* **363** 56–8
[4] Gao L, Xue Y Y, Chen F, Xiong Q, Meng R L, Ramirez D, Chu C W, Eggert J H and Mao H K 1994 *Phys. Rev.* B **50** 4260–3
[5] Kuzemskaya I G, Kuzemsky A L and Cheglokov A A 2000 *J. Low Temp. Phys.* **118** 147–52
[6] Wang Y Q, Meng R l, Sun Y Y, Ross K, Huang Z J and Chu C W 1993 *Appl. Phys. Lett.* **63** 3084–6
[7] Tsuei C C, Gupta A, Trafas G and Mitzi D 1994 *Science* **263** 1259–61
[8] Yun S H *et al* 1995 *Appl. Phys. Lett.* **67** 2866–8
[9] Yun S H and Wu J Z 1996 *Appl. Phys. Lett.* **68** 862–4
[10] Yun S H, Pedarnig J D, Rössler R, Bäuerle D and Obradors X 2000 *Appl. Phys. Lett.* **77** 1369–71
[11] Ogawa A, Sugano T, Wakana H, Kamitani A, Adachi S, Tarutani Y and Tanabe K 2004 *Japan. J. Appl. Phys.* **43** L40–3
[12] Harris J M, Wu H, Ong N P, Meng R L and Chu C W 1994 *Phys. Rev.* B **50** 3246–9
[13] Sun Y, Guo J D, Wang Y and Xiong G C 2001 *Supercond. Sci. Technol.* **14** 607–10
[14] Kang W, Yun S, Wu J and Kim D 1997 *Phys. Rev.* B **55** 621–5
[15] Kang W N, Kang B W, Chen Q Y, Wu J Z, Bai Y, Chu W K, Christen D K, Kerchner R and Lee S I 2000 *Phys. Rev.* B **61** 722–6
[16] Salem A, Jakob G and Adrian H 2004 *Physica* C **402** 354–64
[17] Salem A, Jakob G and Adrian H 2004 *Physica* C **415** 62–8
[18] Richter H, Puica I, Lang W, Peruzzi M, Durrell J H, Sturm H, Pedarnig J D and Bäuerle D 2006 *Phys. Rev.* B **73** 184506
[19] Chan M K *et al* 2014 *Phys. Rev. Lett.* **113** 177005
[20] Pelc D, Anderson Z, Yu B, Leighton C and Greven M 2019 *Nat. Commun.* **10** 2729
[21] Bäuerle D 2000 *Laser Processing and Chemistry* 3rd edn (Berlin: Springer)
[22] Pedarnig J D *et al* 2010 *Thin Solid Films* **518** 7075–80
[23] Lang W, Heine G, Schwab P, Wang X Z and Bäuerle D 1994 *Phys. Rev.* B **49** 4209–17
[24] Wang X Z, Hellebrand B, Bäuerle D, Strecker M, Wortmann G and Lang W 1995 *Physica* C **242** 55–62
[25] Lang W and Pedarnig J D 2010 Ion irradiation of high-temperature superconductors and its application for nanopatterning *Nanoscience and Engineering in Superconductivity*, eds V Moshchalkov, R Wördenweber and W Lang (Heidelberg: Springer) pp 81–104

[26] Larkin A and Varlamov A 2005 *Theory of Fluctuations in Superconductors* (Oxford: Clarendon) (https://doi.org/10.1093/acprof:oso/9780198528159.001.0001)
[27] Solovjov A L and Dmitriev V M 2009 *Low Temp. Phys.* **35** 169–97
[28] Sekirnjak C, Lang W, Proyer S and Schwab P 1995 *Physica* C **243** 60–8
[29] Aslamazov L and Larkin A 1968 *Sov. Phys.-Solid State* **10** 875–80
[30] Lawrence W E and Doniach S 1971 Theory of layer structure superconductors *Proc. 12th Int. Conf. on Low Temperature Physics* ed E Kanda (Keigaku) pp 361–2
[31] Radaelli P G, Wagner J L, Hunter B A, Beno M A, Knapp G S, Jorgensen J D and Hinks D G 1993 *Physica* C **216** 29–35
[32] Lang W, Göb W, Kula W and Sobolewski R 1995 *Z. Phys.* B **98** 453–6
[33] Hikami S and Larkin A 1988 *Mod. Phys. Lett.* **2** 693–8
[34] Ikeda R, Ohmi T and Tsuneto T 1989 *J. Phys. Soc. Japan* **58** 1377–86
[35] Ullah S and Dorsey A 1991 *Phys. Rev.* B **44** 262–73
[36] Lang W 1994 *Physica* C **226** 267–78
[37] Carballeira C, Curras S R, Vina J, Veira J A, Ramallo M V and Vidal F 2001 *Phys. Rev.* B **63** 144515
[38] Leridon B, Dfossez A, Dumont J, Lesueur J and Contour J P 2001 *Phys. Rev. Lett.* **87** 197007
[39] Puźniak R, Usami R, Isawa K and Yamauchi H 1995 *Phys. Rev.* B **52** 3756–64
[40] Thompson J R, Ossandon J G, Christen D K, Paranthaman M, Specht E D and Kim Y C 1996 *Phys. Rev.* B **54** 7505–11
[41] Huang Z J, Xue Y Y, Meng R L, Qiu X D, Hao Z D and Chu C W 1994 *Physica* C **228** 211–5
[42] Le Bras G, Fruchter L, Vulcanescu V, Viallet V, Bertinotti A, Forget A, Hammann J, Marucco J F and Colson D 1996 *Physica* C **271** 205–13
[43] Vulcanescu V, Fruchter L, Bertinotti A, Colson D, Le Bras G and Marucco J F 1996 *Physica* C **259** 131–4
[44] Lang W, Heine G, Kula W and Sobolewski R 1995 *Phys. Rev.* B **51** 9180–92
[45] Lang W, Göb W, Pedarnig J D, Rössler R and Bäuerle D 2001 *Physica* C **364–5** 518–21
[46] Ao P 2020 *Phys. Rev. Lett.* **124** 249701
[47] Zhao S Y F *et al* 2020 *Phys. Rev. Lett.* **124** 249702
[48] Puica I, Lang W, Göb W and Sobolewski R 2004 *Phys. Rev.* B **69** 104513 and references therein
[49] Ao P 1998 *J. Phys.: Condens. Matter* **10** L677–82
[50] Kopnin N B and Vinokur V M 1999 *Phys. Rev. Lett.* **83** 4864–7
[51] D'Anna G, Berseth V, Forró L, Erb A and Walker E 1998 *Phys. Rev. Lett.* **81** 2530–3
[52] Göb W, Liebich W, Lang W, Puica I, Sobolewski R, Rössler R, Pedarnig J D and Bäuerle D 2000 *Phys. Rev.* B **62** 9780–3
[53] Anderson P W 1991 *Phys. Rev. Lett.* **67** 2092–4
[54] Volger J 1950 *Phys. Rev.* **79** 1023–4